Observation of the Second Harmonic in Thomson Scattering from Relativistic Electrons

Marcus Babzien, Ilan Ben-Zvi, Karl Kusche, Igor V. Pavlishin, Igor V. Pogorelsky, David P. Siddons, and Vitaly Yakimenko
Brookhaven National Laboratory, Upton, New York 11973, USA

David Cline and Feng Zhou
University of California at Los Angeles, Los Angeles, California 90095, USA

Tachishige Hirose
Waseda University, Shinjuku-ku, Tokyo 169-8555, Japan

Yoshio Kamiya and Tetsuro Kumita
Tokyo Metropolitan University, Hachioji, Tokyo 192-0397, Japan

Tsunehiko Omori, Junji Urakawa, and Kaoru Yokoya
High Energy Accelerator Research Organization, Tsukuba, Ibaraki 305-0801, Japan
(Received 24 May 2005; published 8 February 2006)

A free relativistic electron in an electromagnetic field is a pure case of a light-matter interaction. In the laboratory environment, this interaction can be realized by colliding laser pulses with electron beams produced from particle accelerators. The process of single photon absorption and reemission by the electron, so-called linear Thomson scattering, results in radiation that is Doppler shifted into the x-ray and γ-ray regions. At elevated laser intensity, nonlinear effects should come into play when the transverse motion of the electrons induced by the laser beam is relativistic. In the present experiment, we achieved this condition and characterized the second harmonic of Thomson x-ray scattering using the counterpropagation of a 60 MeV electron beam and a subterawatt CO_2 laser beam.

DOI: 10.1103/PhysRevLett.96.054802 PACS numbers: 41.50.+h, 41.75.Ht, 42.55.Lt

The process of a linear Thomson scattering predominates at relatively moderate laser intensities. Such scattering generates near-monochromatic and well-collimated radiation that is Doppler-shifted into the x- and γ-ray regions. A series of proof-of-principle experiments [1–4] brought Thomson scattering x-ray sources to the verge of opening up new fields of application. Such potential applications include medical and biological imaging, picosecond and femtosecond x-ray microscopy and holography, dynamic analysis of chemical reactions, phase transitions, and other ultrafast processes traced to atomic precision [5–7]. In nuclear- and high-energy physics, an identical mechanism named Compton scattering can be utilized for prospective positron injectors [8], and γ-γ or γ-lepton colliders [9,10]. Note that the process is called Thomson scattering if the energy of the produced photon is much less than the electron energy, i.e., $h\nu \ll \gamma m_e c^2$, where γ is the Lorentz factor, e is the electron charge, and m_e is the electron mass. Otherwise, it is called Compton scattering.

The spectrum and angular pattern of the scattered radiation become more complex when the laser intensity reaches a level where there is an appreciable probability of simultaneous multiphoton absorption by free electrons and the emission of single photons of higher energy. In classical language, nonlinear effects come into play when the transverse motion of the electrons induced by the laser beam is relativistic. The onset of a nonlinear regime usually is characterized by the laser strength parameter $a_0 = eE/m_e\omega_L c$ approaching or exceeding unity, where E is the amplitude of laser's electric field, ω_L is the laser frequency, and c is the light phase velocity. Nonlinear Thomson scattering has been studied theoretically since the 1960s in the frameworks of classical [11–16], semiclassical [17,18], and quantum theories [19–21]. The theoretical works give us a comprehensive understanding of the spectral- and angular-intensity distributions of Thomson harmonics for arbitrary laser intensity, polarization, and interaction angles [14].

In previous nonlinear Thomson scattering experiments, the second-harmonic radiation first was observed during the interaction of a Q-switched Nd:YAG laser ($a_0 = 0.01$) with 1 keV electrons [22], and later it was studied while interacting a mode-locked Nd:YAG laser ($a_0 = 2$) with plasma electrons [23]. Researchers at the Stanford Linear Accelerator observed a nonlinear energy shift in the spectrum of electrons scattered off a high-energy (~50 GeV) electron beam (e-beam) using a terawatt Nd:glass laser with ($a_0 = 0.6$) [24]. However, the detection of the scattered γ radiation has not been attempted. Thus, until now, theoretical predictions regarding nonlinear Thomson scat-

 © 2006 The American Physical Society

tering of electromagnetic (EM) radiation lacked experimental verification in the x-ray domain attainable with relativistic e-beams.

In the present experiment, the counterpropagation of a 60 MeV e-beam and a subterawatt CO_2 laser beam of $a_0 \approx 0.35$ allowed us to take single-shot measurements of the angular distribution of intensity in the second harmonic of Thomson scattered x rays above 6.5 keV energy and at various laser polarizations.

Let us look at a physical origin of the fundamental and the second-harmonic components of EM radiation backscattered from a relativistic free electron. For this purpose, the classical picture of Thomson scattering [11–16] is suitable. In the electron rest frame moving at velocity βc inside a counterpropagating laser EM field with a wave number $k = 2\pi c/\omega_L$, the EM wave appears at a double frequency, $2\omega_L$. This forces the electron to oscillate along the electric field $\vec{E}$ and emit synchrotron radiation at the same basic frequency, $2\omega_L$. A two-lobe $\sin^2\theta$ polar angular distribution of the resulting dipole radiation is oriented symmetrically along the $\vec{k}$ vector. However, an ''observer'' positioned in the laboratory frame detects backscattered radiation at the frequency $\omega = 2\omega_L/(1-\beta) \approx 4\gamma^2\omega_L$ (the Doppler blueshift). Hence, starting with a 60 MeV e-beam ($\gamma = 120$) and a CO_2 laser beam of wavelength $\lambda_L = 10.6$ μm, we obtain backscattered photons in the x-ray region with $\lambda = \lambda_L/4\gamma^2 = 1.7$ Å, corresponding to 6.5 keV. This observer can see backscattered light only when a projection of the phase velocity onto the direction of the electron propagation is larger than βc, i.e., when it is within the apex angle $\theta \geq \cos^{-1}\beta$. Using the expansions $\cos\theta \approx 1 - \frac{1}{2}\theta^2$ and $\beta = \sqrt{1-1/\gamma^2} \approx 1 - 1/2\gamma^2$, the angular divergence of the backscattered radiation is $\theta = 1/\gamma$.

The second-order correction to the electron's motion is due to the $\vec{v} \times \vec{B}$ coupling that forces the electron to oscillate along the $\vec{k}$ vector at the double basic frequency $4\omega_L$. Therefore, it produces the $\cos^2\theta$ intensity distribution oriented perpendicular to $\vec{k}$. The combined electron trajectory in the relativistic frame forms a figure-of-eight pattern [12,25]. In the laboratory frame, the $\cos^2\theta$ distribution appears tipped forward and develops two maxima oriented along the laser polarization axis with an angular separation $1/\gamma$. Lorentz transformation results in 13 keV x-ray energy.

Still higher order perturbations of the electron's orbit must be considered as the laser intensity becomes ultrarelativistic ($a_0 \gg 1$). Then, there is a more complex radiation distribution consisting of multiple harmonics along with spectral expansion into the hard–x-ray region. However, under our experimental condition $a_0 \approx 0.35$, only the fundamental- and the second-harmonic contributions are important.

Figure 1 depicts a principle diagram of the present experiment. The typical input parameters for the electron and CO_2 laser beams are as follows: Electron beam energy 60 MeV, bunch charge 0.5 nC, duration 3.5 psec (FWHM), transverse dimensions at the interaction point 45 μm $\times$ 80 μm (rms); laser pulse energy 4 J, duration 30 psec (FWHM), and focal spot size 30 μm (rms). The laser pulse introduced into the e-beam line through a salt (KCl) window is reflected along the e-beam direction by a flat Cu mirror tilted at a 45° angle, and is focused head-on to the e-beam with a normal-incidence parabolic mirror with the ratio of the equivalent focal length to the diameter $f/\# = 1$. Both mirrors have central holes drilled along the e-beam axis to transmit the e-beam and the generated x rays.

A narrow cone of x rays generated from the interaction area passes through the 2 mm hole in the parabolic mirror and is extracted from the e-beam line through a 250 μm thick beryllium (Be) vacuum window. Spent electrons, deflected by the 90° dipole magnet, do not reach the Be window. This allows one to minimize parasitic bremsstrahlung noise on x-ray detectors positioned behind the window. To image the transverse intensity profile of the x-ray beam, we used a luminescent screen (Kodak-2854) viewed with a CCD camera, along with a wide-aperture silicon (Si) diode for measuring the integral x-ray yield. Inserting the 10 μm thick Ag foil in front of the detector allowed us to cut off low-energy x rays produced in the linear (single photon) process and visualize the nonlinear component in the Thomson scattering.

Note that a conventional x-ray spectrometer based on the Bragg reflection from a crystal proved to be unsuitable for

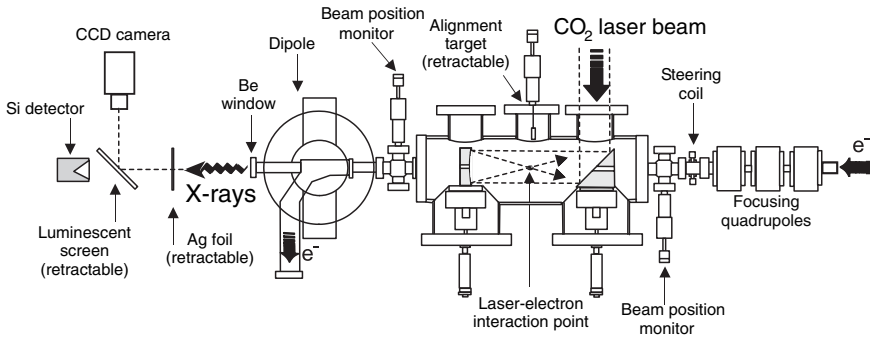

FIG. 1. A diagram of the experiment.

this study, which was conducted within a strong bremsstrahlung environment caused by a relativistic e-beam. Also, we could not investigate polarization-dependent angular distributions in nonlinear Thomson scattering, one of the main motivations for this experiment, with a conventional spectrometer.

To accurately and quantitatively predict and process the experimental results, we undertook Monte Carlo simulations using the computer code CAIN [26] based on the Volkov solutions to the Dirac equation. This code allows calculating the quantum transition rate of photon emission from electrons in a high EM field assuming Gaussian temporal and spatial distributions of the focused electron and laser beams.

Figure 2 shows the x-ray spectra simulated for our experimental conditions. The black line is the radiation spectrum at the interaction point. The energy of photons produced by the linear Thomson scattering process is limited to $4\gamma^2\hbar\omega_L = 6.5$ keV, but the nonlinear process extends the spectrum into the hard–x-ray region. The solid red line shows the x-ray spectrum at the detector's location outside the vacuum beam line and after attenuation in air and at the Be window. The solid blue line shows the x-ray spectrum filtered by the 10 μm Ag foil. Bulk x rays produced in the linear Thomson scattering are stopped on the foil, and the nonlinear contribution is highlighted. Dashed lines in Fig. 2 show x-ray transmission of the Be window and air (red line) and the Ag foil (blue line) used in the simulation.

The total x-ray flux is measured with the Si diode and compared with the number of photons evaluated from the computer simulation. We found that the maximum deposited x-ray dose in a single shot was 1.1×10^{11} eV.

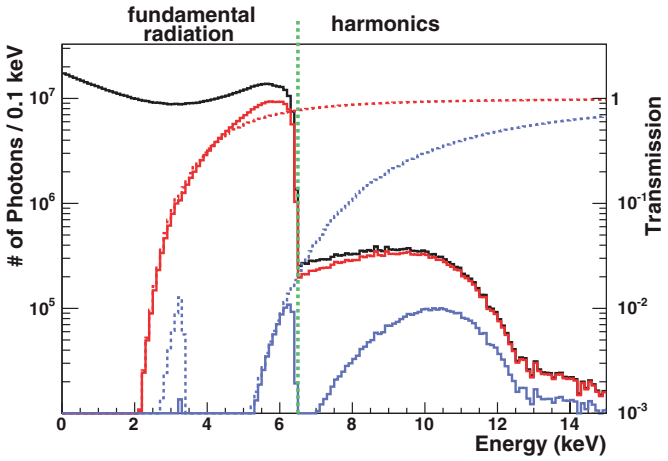

FIG. 2 (color). Simulated energy spectra of Thomson x rays. Solid lines: (black line) at the interaction point; (red line) on the detector after attenuation in the Be window and air; (blue line) filtered by a 10 μm Ag foil. Dashed lines show combined spectral transmission of the Be window with air (red line) and Ag foil (blue line). A green line shows the high-energy edge (6.5 keV) for the linear Thomson scattering.

Notably, the obtained x-ray yield of 2×10^7 photons is among the highest ever reported from laser-driven Thomson scattering experiments. Blocked with the Ag filter, the signal dropped to 2.6×10^9 eV. This reduction, by a factor of 40, corresponds to the ratio of the energy integrals under the simulated red and blue curves in Fig. 2. We note that tuning the laser pulse to 200 ps with the resulting 10 times reduction in the peak intensity at the same laser energy does not greatly affect the fundamental signal but completely washes out the filtered signal ($>$6.5 keV). This finding confirms the nonlinear dependence of the high-energy component in the x-ray spectrum upon the laser intensity. Note that background due to bremsstrahlung photons from the e-beam was detected with the laser beam off. Typical bremsstrahlung energy deposit on the Si detector was 1.3×10^9 eV and is subtracted to measure Thomson scattering signals shown above.

Figure 3 displays the transverse profiles of Thomson x rays observed on a luminescent screen. A two-peak pattern clearly had developed after spectral filtering and was oriented along the axis of the laser polarization. The distance measured across the screen between the peaks corresponds to 6 mrad in the polar-angle distribution; this value is consistent with the $1/\gamma$ estimate and, especially, with more comprehensive CAIN simulations that account for the narrowing of the transverse profile due to preferential filtering of the low-energy peripheral x rays. We also experimentally confirmed a similar $1/\gamma$ divergence for the single-lobe fundamental x-ray beam. Figure 4 gives a comparison between the experimental and simulated polar distributions plotted in the plane of the laser polarization.

Finally, we took images of the transverse x-ray profiles for different polarizations of the CO_2 laser. We rotated the linear polarization through 90°, and then converted it to a circular one by inserting a half-wave plate and a quarter-wave plate into the laser beam, respectively. Figure 5(a) shows the clear 90° rotation of the azimuthal distribution of the filtered high-energy x rays for a linearly polarized laser. Similarly, converting the CO_2 laser beam to a circular polarization results in an azimuthally symmetric circular

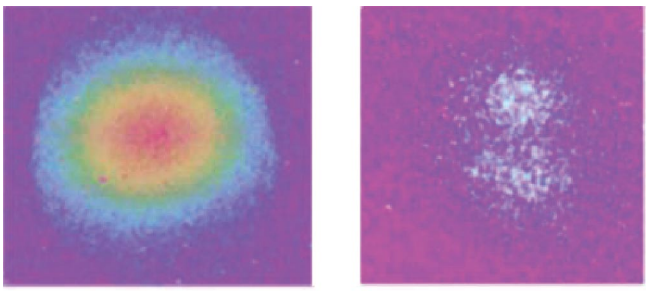

(a) (b)

FIG. 3 (color). X-ray images observed on a luminescent screen: (a) without the Ag foil, and (b) with the 10 μm Ag foil filter.

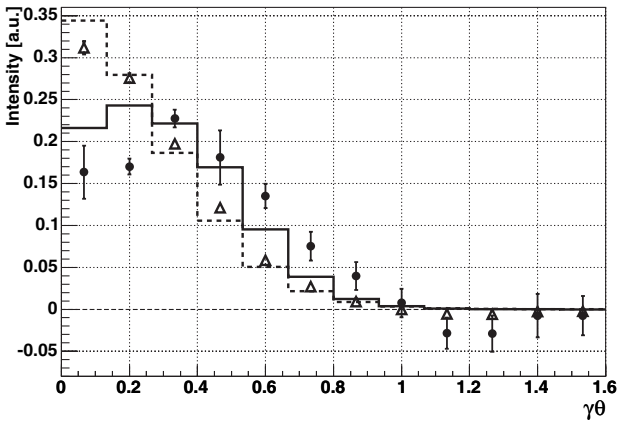

FIG. 4. Polar distributions of the scattered x-ray intensity in the plane of laser polarization. Dashed line and triangles: correspondingly simulation and experimental points for unfiltered x-ray signal; solid line and circles with error bars: correspondingly simulation and experimental points obtained with the 10 μm Ag foil filter.

pattern [Fig. 5(b)] as the semiclassical theory of Thomson scattering predicts [17,18].

Thus, our observations of transverse x-ray distributions produced via the nonlinear Thomson scattering in a head-on collision of laser and relativistic electron beams validate theoretical predictions in the strong EM field regime.

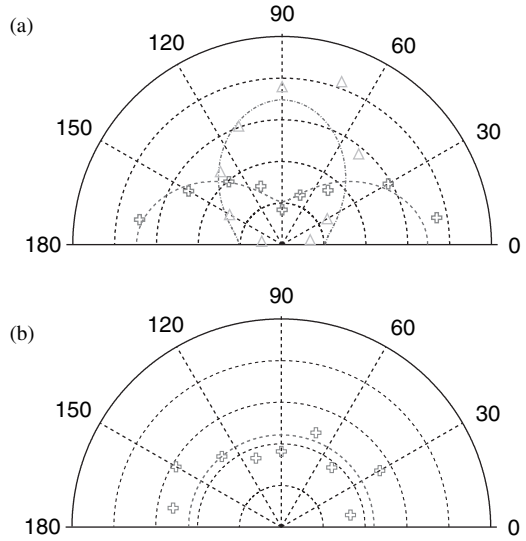

FIG. 5. Azimuthal distribution of the x-ray intensity in the second harmonic of Thomson scattering filtered out after passing through Be window and Ag foil. Crosses and triangles: experimental points; lines: simulations. (a) Obtained with a linear polarized laser (crosses and triangles correspond to two orthogonal directions of the laser polarization). (b) Obtained with a circular polarized laser.

We thank K. McDonald, Z. Segalov, A. Tsunemi, A. Endo, and other colleagues who contributed to initiating this study, W. Leemans for advising on diagnostics, and M. Woodle, D. Davis, and J. Skaritka for their technical support. The work was supported by the Japan-USA Collaborative Research Grant, Grant-in-Aid for Scientific Research from the Japan Society for the Promotion of Science and by the Offices of High Energy Physics and Basic Energy Science, U.S. DOE.

[1] W. P. Leemans *et al.*, Phys. Rev. Lett. **77**, 4182 (1996).
[2] M. Uesaka *et al.*, Nucl. Instrum. Methods Phys. Res., Sect. A **455**, 90 (2000).
[3] A. Ting *et al.*, J. Appl. Phys. **78**, 575 (1995).
[4] I. V. Pogorelsky *et al.*, Phys. Rev. ST Accel. Beams **3**, 090702 (2000).
[5] D. Attwood, *Soft X-rays and Extreme Ultraviolet Radiation: Principles and Applications* (Cambridge University Press, Cambridge, 1999).
[6] R. W. Schoenlein *et al.*, Science **274**, 236 (1996).
[7] C. J. Joshi and P. B. Corkum, Phys. Today **48**, No. 1, 36 (1995).
[8] T. Omori *et al.*, Nucl. Instrum. Methods Phys. Res., Sect. A **500**, 232 (2003).
[9] V. I. Telnov, Nucl. Instrum. Methods Phys. Res., Sect. A **294**, 72 (1990).
[10] C. E. Clayton, N. A. Kurnit, and D. D. Meyerhofer, Nucl. Instrum. Methods Phys. Res., Sect. A **355**, 121 (1995).
[11] Vachaspati, Phys. Rev. **128**, 664 (1962).
[12] E. S. Sarachik and G. T. Schappert, Phys. Rev. D **1**, 2738 (1970).
[13] E. Esarey, S. K. Ride, and P. Sprangle, Phys. Rev. E **48**, 3003 (1993).
[14] S. K. Ride, E. Esarey, and M. Baine, Phys. Rev. E **52**, 5425 (1995).
[15] Y. Y. Lau, F. He, D. P. Umstadter, and R. Kowalczyk, Phys. Plasmas **10**, 2155 (2003).
[16] A. K. Puntajer and C. Leubner, J. Appl. Phys. **67**, 1606 (1990).
[17] L. S. Brown and T. W. B. Kibble, Phys. Rev. **133**, A705 (1964).
[18] D. Li, K. Yokoya, T. Hirose, and R. Hamatsu, Jpn. J. Appl. Phys. **42**, 5376 (2003).
[19] Z. Fried and J. H. Eberly, Phys. Rev. **136**, B871 (1964).
[20] L. M. Frantz, Phys. Rev. **139**, B1326 (1965).
[21] E. Ugaz, Phys. Rev. A **50**, 34 (1994).
[22] T. J. Englert and E. A. Rinehart, Phys. Rev. A **28**, 1539 (1983).
[23] S.-Y. Chen, A. Maksimchuk, and D. Umstadter, Nature (London) **396**, 653 (1998).
[24] C. Bula *et al.*, Phys. Rev. Lett. **76**, 3116 (1996).
[25] J. D. Jackson, *Classical Electrodynamics* (John Wiley & Sons, Inc., New York, 1998), 3rd ed.
[26] P. Chen *et al.*, Nucl. Instrum. Methods Phys. Res., Sect. A **355**, 107 (1995).